Using a Large Space-Variant Beamformer for Multistatic SAR Imaging

Thomas Kraus, Gerhard Krieger, Markus Bachmann, Alberto Moreira
Microwaves and Radar Institute, German Aerospace Center (DLR), Oberpfaffenhofen, Germany, t.kraus@dlr.de

Abstract

Multistatic synthetic aperture radar (SAR) imaging is a promising candidate for future Earth observation missions. On the one hand, the multichannel concept enables high azimuth resolution while acquiring wide swathes. On the other hand, the use of many small satellites provides the benefits of cost efficient mass manufacturing and graceful degradation which reduces the effort for redundancy on the single platforms. One of the key challenges is the processing of the SAR data of many distributed channels to a single high-resolution image. Compared to single platform multichannel systems, the phase centers are no longer aligned in azimuth direction, but baselines in cross-track and line-of-sight direction are inevitable. Additionally, the sampling in along-track is also a function of the formation and the used pulse repetition frequency (PRF). Several approaches for the processing have been investigated in literature. The paper in hand investigates a beamforming approach and discusses its benefits and limitations.

1 Introduction

There is a growing demand for high-resolution wide-swath (HRWS) SAR imaging as it has proven to be an irreplaceable source of information for scientists, commercial, and governmental users. An example demanding wide coverage and high resolution at the same time is ship detection and oil spill monitoring over wide areas. The high resolution imaging of the detected ships might be of interest for further identification. To overcome the contradicting PRF requirements imposed by the simultaneous demand for high azimuth resolution and wide coverage, innovative techniques have been suggested. The multi-channel concept proposed in [1] can be seen as the starting point. This concept is generalized in [2] for non-uniform sampling conditions and further elaborated, e.g., in [3], [4], [5]. A demonstration of the technique on TerraSAR-X is reported in [6]. Further research focused on distributed satellite systems. A formation with large along-track baselines is discussed in [7]. Systems with cross-track baselines can additionally provide interferometric and tomographic capabilities as discussed in [8], [9]. First results for distributed SAR imaging are reported in [10], [11], [12]. For multistatic SAR systems the presence of cross-track baselines offers new opportunities as the generation of a digital elevation model (DEM) in a single overflight [13]. For a HRWS application, however, these baseline components are complicating the azimuth signal reconstruction process. A phase difference between the channels is introduced depending on the orbital parameters and the imaged topography. Several compensation methods used for a TerraSAR-X and TanDEM-X experiment are discussed in [14] and further elaborated in [15]. Another approach compensating the cross-track baseline signal and employing the traditional reconstruction method is discussed in [16]. The paper in hand concentrates on the beamforming method, further develops the underlying ideas, and shows the potential of the method as well as its limitations.
The paper is structured as follows. In section 2 the signal model and the simulation assumptions are introduced. Section 3 describes the investigated approaches. Simulation results are shown in section 4 and section 5 concludes the paper.

2 System Parameters

We assume a system with several satellites in close orbit formation where one satellite is actively transmitting and all platforms are receiving. **Figure 1** shows the geometry under consideration for the example of a three-channel system where the crosses on the orbit tracks already depict the equivalent phase centers. The crosses on the ground represent the location of pixels in the final image. The position of a point target in the center of the aperture is highlighted by a red star. The positions where the first order ambiguities are expected to appear for this target according to the used PRF are highlighted with yellow stars. The distance between each of the considered M phase centers to N pixels on the ground is denoted d_{ij}. For the simulations a rectilinear geometry is assumed taking TerraSAR-X system parameters as a basis, e.g., an orbit altitude of 512 km and an azimuth antenna size of 4.8 m for the X-band system. An overview is given in **Table 1**.

Table 1: System parameters for the simulation

Parameter	Value
radar frequency	9.65 GHz
orbit altitude	512 km
antenna size (azimuth)	4.8 m
look angle	45 °
terrain slope (azimuth)	2 %

The main challenges of the distributed SAR system are the sensitivity to topography both in range and azimuth direction due to the presence of a cross-track baseline. The topography is modeled as a slope in azimuth direction. If not otherwise noted, we assume a slope of 2%. The formation of the satellites is described via the baselines as discussed in [17]. Additionally, the sampling conditions in along track are driven by the along-track baseline and the assumed PRF.

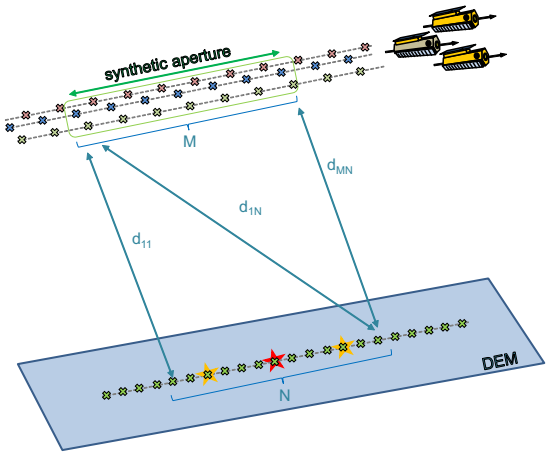

Figure 1: Sketch of the acquisition geometry and the processing for the beamforming approach for a three-channel system. The length of the synthetic aperture comprising M samples is highlighted. The distances d_{ij} of the M samples to N pixels on ground are used to calculate the beamformer weights. The target to be focused is shown in red and its ambiguities in yellow.

3 The Beamforming Approach

The well established back-projection technique can be regarded either as a matched filter or as a kind of beamforming and serves as a reference for comparing the results of the proposed beamformer. It maximizes the signal energy for a given point target on the ground [18]. However, it does not provide any means to control the ambiguity performance. Therefore, more sophisticated beamforming techniques have to be considered [19], [20], [8]. The goal is to steer nulls to the positions of the ambiguities depicted in yellow.
The array manifold vector $\mathbf{m}$ describes the spatial characteristics of the array, i.e. the synthetic aperture, with respect to a point target on the ground. The array manifold vectors for different ground targets can be collected in a matrix

$$\mathbf{M} = [\mathbf{m}_1, ..., \mathbf{m}_N] = \left[\mathrm{e}^{\frac{j4\pi d_{i,j}}{\lambda}}\right] . \quad (1)$$

The maximum likelihood (ML) beamformer

$$\mathbf{W}_{\mathrm{ML}} = (\mathbf{M}^{\mathrm{H}}\mathbf{K}_{\mathrm{n}}^{-1}\mathbf{M})^{-1}\mathbf{M}^{\mathrm{H}}\mathbf{K}_{\mathrm{n}}^{-1} , \quad (2)$$

as proposed in [19] was used as a starting point. Here $\mathbf{W}_{\mathrm{ML}}$ is the weights matrix containing N weight vectors for the considered targets on the ground and $(\cdot)^{\mathrm{H}}$ denotes the conjugate transpose operation. Assuming independent noise samples and therefore a diagonal noise covariance matrix $\mathbf{K}_{\mathrm{n}}$, the weight calculation simplifies to

$$\mathbf{W}_{\mathrm{ML}} = \mathbf{M}^{+} , \quad (3)$$

where $\mathbf{M}^{+}$ denotes the pseudo inverse operation of the in general non-square matrix $\mathbf{M}$. This beamformer is supplemented with a distortion-less constraint and can be described by

$$\mathbf{w} = \mathbf{M}^{+}\mathbf{b} , \quad (4)$$

where $\mathbf{b}$ is the constraint vector with the distortion-less constraint towards the intended point target and nulls towards the ambiguous directions, forming a linear constrained minimum variance (LCMV) beamformer.

Another option would be to suppress the ambiguous power below a certain level, e.g., the noise level, using a sidelobe-constrained minimum variance beamformer [21]. Both techniques result in an azimuth-variant SAR focusing that resembles a large space-variant beamformer, where the beamformer weights are continuously adjusted in accordance with the satellite formation geometry and the terrain topography. The goal is to maximize the energy from a given resolution cell under the constraint of minimizing the signal returns from all other directions, especially from where the ambiguities are expected.

4 Simulation Results

In the following simulation results concerning the impact of the baselines and the topography are shown for a three channel system and the parameters described in section 2.

In **Figure 2** the beamformer pattern derived for both, the beamforming and the back-projection approach are shown for comparison. The beamformer pattern was derived using several (here 31) nulls steered to the ambiguous direction as suggested in [21]. This measure clearly suppresses the return from the ambiguous direction.

The impulse response function for the red target marked in Figure 1 is shown in **Figure 3**. The absence of the first order ambiguity is clearly visible at about 3 km from the main IRF. The second order ambiguity located at about 6 km is dominating the performance but with a much lower power than the first order ambiguity would have had. For back-projection (not shown) the first order ambiguity is present as it cannot be suppressed and has a power of only 10 dB below the peak of the IRF.

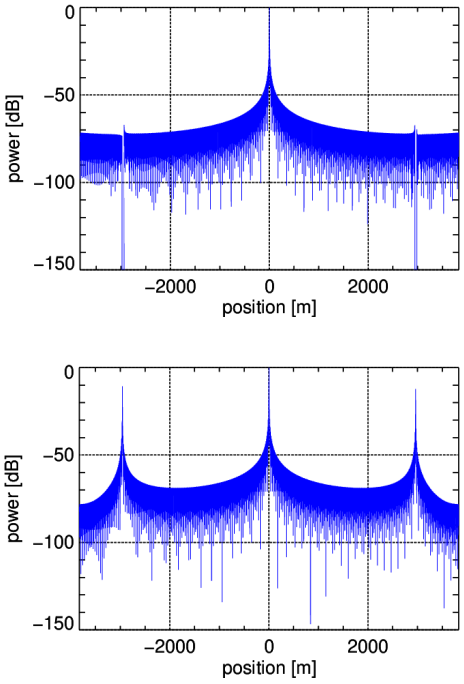

Figure 2: Beamformer patterns derived for a three channel system with 40 m of perpendicular baseline acquiring over a scene with 2% slope in azimuth direction. The PRF of 2 kHz is leading to a uniform sampling in azimuth direction. On the top the pattern derived by the beamformer is depicted. The nulls in the ambiguity direction are clearly visible around position -3000 m and 3000 m. For comparison the pattern of the back-projection approach is depicted on the bottom. The ambiguous directions are clearly visible with a high gain of only about 10 dB below the main impulse response function

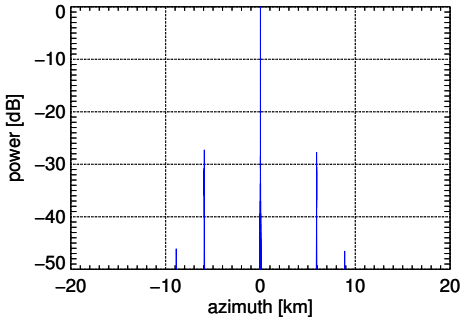

Figure 3: Impulse response function achieved using the beamforming approach.

In **Figure 4** the same geometry but with a different PRF of 1800 Hz instead of 2000 Hz as in the previous simulation is assumed. This leads to a non-uniform sampling in along-track direction which is regarded as a more complex reconstruction scenario. Compared to Figure 2 the ambiguous position is closer to the main IRF as the PRF is lower. Additionally, the beamformer cannot suppress the ambiguity completely any more. Even though the beamformer pattern shows higher gain at the ambiguous regions, the overall performance is not affected by the first order ambiguity. The reason is the dominant power of the second order ambiguity as shown in Figure 3.

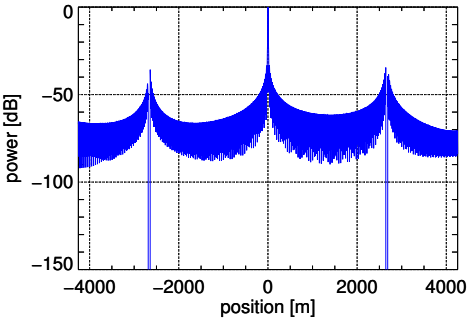

Figure 4: Beamformer pattern derived for a three channel system with 40 m of perpendicular baseline acquiring over a scene with a slope of 2% in azimuth direction. The PRF of 1.8 kHz is leading to a non-uniform sampling in azimuth direction deteriorating the pattern compared to the uniform sampling as shown in Figure 2.

Overall the azimuth ambiguity-to-signal ratio (AASR) performance is depending on the PRF. In **Figure 5** the AASR is shown versus the PRF for a three satellite system with 40 m of perpendicular baseline acquiring over a scene with a slope of 2% in azimuth direction. The red and the orange curve represent the AASR to the left and to the right of the main IRF position, respectively. The performance is the same towards both sides and it is improving for higher PRFs. Even though a PRF of 2.0 kHz represents the uniform sampling case in azimuth, no optimum can be observed but the trend is unchanged for higher PRFs. An AASR of better than -25 dB can be achieved for PRFs larger than 2.05 kHz. For comparison the AASR for a single channel is shown in blue and the performance for an equivalent system with one channel but triple PRF is depicted in green as the benchmark system.

For a scenario with perpendicular baseline and topography in azimuth direction the degradation of the AASR performance is symmetric as shown in Figure 5. Assuming a line-of-sight (LOS) baseline instead, the performance is not symmetric any more, as depicted in **Figure 6**. Especially for PRFs below the uniform sampling PRF of 2.0 kHz the AASR is degrading asymmetrically. Nevertheless, a high AASR performance of better than -25 dB is achieved for PRFs larger than 1.9 kHz.

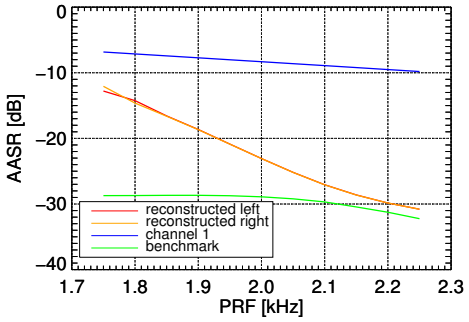

Figure 5: AASR versus PRF for a three satellite system with 40 m perpendicular baseline acquiring over a scene with a slope of 2% in azimuth direction.

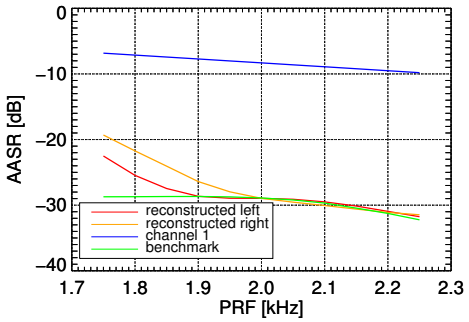

Figure 6: AASR versus PRF for a three satellite system with 40 m line-of-sight baseline acquiring over a scene with a slope of 2% in azimuth direction.

5 Conclusions

The paper addresses an innovative approach for the processing of multistatic SAR data. The method is treating the SAR processing as a large space-variant beamformer, offering unprecedented flexibility in designing the pattern. The positions, where in nominal SAR processing ambiguities are expected can be nulled by the beamformer, whereas the main response of the IRF can be preserved by a distortion-less constraint. The impact of cross-track baselines and terrain topography are discussed and it is shown that a high AASR performance can be achieved.

References

[1] A. Currie and M. A. Brown, "Wide-swath SAR," in *Proc. Inst. Elect. Eng.—Radar, Sonar, Navigat.*, vol. 139, no. 2, 1992, pp. 122–135.

[2] G. Krieger, N. Gebert, and A. Moreira, "Unambiguous SAR signal reconstruction from nonuniform displaced phase center sampling," *IEEE Geosci. Remote Sens. Lett.*, vol. 1, no. 4, pp. 260–264, 2004.

[3] N. Gebert, G. Krieger, and A. Moreira, "Digital beamforming on receive: Techniques and optimization strategies for high-resolution wide-swath SAR imaging," *IEEE Trans. Aerosp. Electron. Syst.*, vol. 45, no. 2, pp. 564–592, 2009.

[4] I. Sikaneta, C. Gierull, and D. Cerutti-Maori, "Optimum signal processing for multichannel SAR: With application to high-resolution wide-swath imaging," *IEEE Trans. Geosci. Remote Sens.*, vol. 52, no. 10, pp. 6095–6109, 2014.

[5] D. Cerutti-Maori, I. Sikaneta, J. Klare, and C. H. Gierull, "MIMO SAR processing for multichannel high-resolution wide-swath radars," *IEEE Transactions on Geoscience and Remote Sensing*, vol. 52, no. 8, pp. 5034–5055, 2014.

[6] J.-H. Kim, M. Younis, P. Prats-Iraola, M. Gabele, and G. Krieger, "First spaceborne demonstration of digital beamforming for azimuth ambiguity suppression," *IEEE Trans. Geosci. Remote Sens.*, vol. 51, no. 1, pp. 579–590, 2013.

[7] N. Sakar, M. Rodriguez-Cassola, P. Prats-Iraola, and A. Moreira, "Azimuth reconstruction algorithm for multistatic SAR formations with large along-track baselines," vol. 58, pp. 1931–1940, 2020.

[8] G. Krieger and A. Moreira, "Potential of digital beamforming in bi-and multistatic SAR," in *Geoscience and Remote Sensing Symposium, 2003. IGARSS'03. Proceedings. 2003 IEEE International*, vol. 1. IEEE, 2003, pp. 527–529.

[9] ——, "Spaceborne bi- and multistatic SAR: potential and challenges," *Proc. Inst. Elect. Eng.—Radar, Sonar, Navigat.*, vol. 153, no. 3, pp. 184–198, 2006.

[10] T. Kraus, B. Bräutigam, M. Bachmann, and G. Krieger, "Multistatic SAR imaging: First results of a four phase center experiment with TerraSAR-X and TanDEM-X," in *Proc. EUSAR*, Hamburg, Germany, 2016.

[11] T. Kraus, M. Bachmann, L. Heiderich, G. Krieger, and A. Moreira, "Multistatic SAR imaging: Comparison of simulation results and experimental data," in *Proc. Inst. Elect. Eng.—Radar, Sonar, Navigat.* IET, 2017.

[12] T. Kraus, G. Krieger, M. Bachmann, and A. Moreira, "Spaceborne demonstration of distributed SAR imaging with TerraSAR-X and TanDEM-X," *IEEE Geosci. Remote Sens. Lett.*, 2019, early access.

[13] M. N. Peixoto, M. Villano, G. Krieger, A. Moreira, and C. Waldschmidt, "A novel technique to generate digital elevation models in a single pass using a cluster of smallsats," in *Proc. IGARSS*, 2023.

[14] T. Kraus, M. Bachmann, and G. Krieger, "Topography correction for distributed SAR imaging: A case study for TerraSAR-X and TanDEM-X," in *Proc. EUSAR*, 2018.

[15] T. Kraus, G. Krieger, M. Bachmann, and A. Moreira, "Addressing the terrain topography in distributed SAR imaging," in *Proc. EUSAR*, 2019.

[16] H. Lin, Y. Deng, H. Zhang, D. Liang, and X. Jia, "An imaging method for spaceborne cooperative multistatic SAR formations with nonzero cross-track baselines," vol. 15, pp. 8541–8551, 2022.

[17] T. Kraus, G. Krieger, M. Bachmann, and A. Moreira, "Formation considerations for distributed satellite SAR systems," in *Proc. EUSAR*, 2021.

[18] L. M. Ulander, H. Hellsten, and G. Stenstrom, "Synthetic-aperture radar processing using fast factorized back-projection," *IEEE Transactions on Aerospace and electronic systems*, vol. 39, no. 3, pp. 760–776, 2003.

[19] N. A. Goodman, S. C. Lin, D. Rajakrishna, and J. M. Stiles, "Processing of multiple-receiver spaceborne arrays for wide-area SAR," *IEEE Trans. Geosci. Remote Sens.*, vol. 40, no. 4, pp. 841–852, 2002.

[20] J. M. Stiles and N. A. Goodman, "Wide area, fine resolution SAR from multi-aperture radar arrays," in *Proc. of the Advanced SAR Workshop*, 2003, p. 10.

[21] H. L. Van Trees, *Optimum array processing: Part IV of detection, estimation, and modulation theory*. John Wiley & Sons, 2004.

[22] N. Sakar, M. Rodriguez-Cassola, P. Prats-Iraola, and A. Moreira, "Polychromatic time domain reconstruction approach for along-track multistatic SAR constellations with varying PRI," in *Proc. European Radar Conf. (EURAD)*, 2020.